



**Synthesis and Li-ion Electrode Properties of Layered MAB
phases Ni_n+1ZnB_n ($n = 1, 2$)**

Journal:	<i>Journal of Materials Chemistry A</i>
Manuscript ID	TA-COM-11-2019-012937.R1
Article Type:	Communication
Date Submitted by the Author:	31-Dec-2019
Complete List of Authors:	Rezaie, Amir A. ; University of California Riverside, Materials Science and Engineering Program Yan, Zheng ; University of California Riverside, Department of Chemical and Environmental Engineering Scheifers, Jan; University of California Riverside, Chemistry Zhang, Jian; University of California Riverside, Materials Science and Engineering Program Guo, Juchen; University of California Riverside, Chemical and Environmental Engineering Fokwa, Boniface; University of California Riverside, Chemistry

Synthesis and Li-ion Electrode Properties of Layered MAB phases $\text{Ni}_{n+1}\text{ZnB}_n$ ($n = 1, 2$)

Amir A. Rezaie,^{a,c} Zheng Yan,^b Jan P. Scheifers,^a Jian Zhang,^c Juchen Guo,^{b,c*} Boniface P. T. Fokwa^{a,c*}

^a Department of Chemistry, University of California, Riverside, 92521 Riverside, CA, USA

^b Department of Chemical and Environment Engineering, University of California, Riverside, 92521 Riverside, CA, USA

^c Materials Science and Engineering Program, University of California, Riverside, 92521 Riverside, CA, USA

*: corresponding authors Emails: bfokwa@ucr.edu, jguo@engr.ucr.edu

Abstract

Ternary MAB phases (layered transition metal borides) have recently attracted interest due to their exfoliation potential toward MBenes (analogous to MXenes), which are predicted to have excellent Li-ion battery performance. We have achieved single-phase synthesis of two MAB phases with general composition $\text{Ni}_{n+1}\text{ZnB}_n$ ($n = 1, 2$), the crystal structures of which contain zinc layers sandwiched between thin ($n = 1$) and thick ($n = 2$) Ni-B slabs. Highly stacked MAB sheets were confirmed by X-ray diffraction and high-resolution scanning electron microscopy for both materials. Exposing $\text{Ni}_{n+1}\text{ZnB}_n$ to diluted hydrochloric acid led to the creation of crystalline microporous structures for $n = 1$ and non-porous detached sheets for $n = 2$. Both morphologies transformed the inactive bulk materials into highly active Li-ion battery anodes with capacities of $\sim 90 \text{ mAh g}^{-1}$ ($n = 1$) and $\sim 70 \text{ mAh g}^{-1}$ ($n = 2$) at a 100 mA g^{-1} lithiation-delithiation rate. The XPS analysis and BET surface area measurements reveal that the increased surface area and the reversible redox reaction of oxidized nickel species are responsible for this drastic increase of the lithiation-delithiation capacity. This proof of concept opens new avenues for the development of porous MAB borides, MAB nanosheets, MBenes and their composites for metal-ion battery applications.

Keywords: Nickel-Zinc Boride, MAB Phase, Porous Microstructure, Li-ion Battery

Since the discovery of MAX phases, these layered transition metal carbides ($X = \text{C}$) and nitrides ($X = \text{N}$) with general formula $\text{M}_{n+1}\text{AX}_n$ ($n = 1-3$) have gained interest among scientists due to their mixed metallic and ceramic properties¹⁻³. These properties include machinability, high corrosion resistance, high ductility, excellent electrical and thermal conductivity, thermal shock resistance, etc⁴⁻⁷. In 2011 Gogotsi et al.⁸ introduced MXenes ($M =$ early transition metal, $X = \text{C}$ or N), which are derived from the MAX phases by chemical exfoliation of the A layer, as promising candidates for lithium-ion battery anodes⁹⁻¹¹. Currently MXenes have been considered for other applications such as batteries⁹⁻¹¹, supercapacitors^{9, 12}, and for magnetic shielding¹³ etc. In 2015, Hillebrecht et al.¹⁴ introduced a MAX-related family of layered materials called MAB phases - MAX phases with $X =$ boron. Even though these MAB phases are chemically and

structurally different from the MAX phases, they have similar properties such as high conductivity¹⁵, stiffness¹⁵ and resistant to thermal shock¹⁶. MAB phases include compounds with different compositions and structures such as M_2AlB_2 ($Cmmm$)¹⁴, $MAIB$ ($Cmcm$)¹⁷, Cr_3AlB_4 ($Immm$)¹⁴, Ru_2ZnB_2 ($I4_1/amd$)¹⁸, Y_2SiB_8 ($P4/mbm$)¹⁹, Cr_5SiB_3 ¹⁶ and Ni_3ZnB_2 ($C2/m$)²⁰⁻²³. The variety of MAB structures differentiate them from the MAX phases which are mainly hexagonal (space group $P6_3/mmc$). This significant structural difference is directed by the boron substructure which varies from dumbbells, to zigzag B_4 fragment, to zigzag boron chain, to chain of boron hexagons and chain of boron double hexagons.¹⁴ In MAX phases, however, no bond exists between X (C, N) atoms. In addition, significant bonding interactions exist between boron and the A atoms in MAB structures, while no significant interaction exist between X and A in MAX structures.²⁴ These significant A-B interactions are likely the main reason why A is rather difficult to be etched out of the MAB structures to produce MBenes²⁵⁻²⁷, while the absence of A-X interactions in MAX phases supports the easy exfoliation of A.²⁴ This analysis shows that exfoliating $Ni_{n+1}ZnB_n$ phases will be as difficult as the other MAB phases. Although no MBene has been realized quantitatively yet, theory has suggested that these materials have great potential in battery and electrocatalysis applications²⁸. Even though several binary transition metal borides such as VB_2 and TiB_2 have been investigated as anodes for non-rechargeable battery systems,^{29,30} the electrochemical properties of MAB phases for rechargeable battery electrodes has not been experimentally investigated, to best of our knowledge.

The structural diversity of MAB phases give them a unique and untapped advantage: Many of them contain M transition elements (spanning the whole 3d spectrum)¹⁴ that are important for Li-ion battery performance: Ti, V, Cr, Fe, Mn and Ni^{31,32}. In this study, we will focus on Ni_2ZnB and Ni_3ZnB_2 , which are evaluated for the first time for their Li-ion electrode properties as a proof of concept. We show that the bulk samples are largely inactive as battery materials, however, exposing Ni_2ZnB and Ni_3ZnB_2 to an acid treatment leads to two unexpected morphological behaviors that drastically increase their Li-ion battery performance.

The Ni-Zn-B system was previously investigated at 800°C by Malik *et al.* showing the existence of different phases such as $Ni_{12}ZnB_8$ (space group: $Cmca$), $Ni_{21}Zn_2B_{20}$ (space group: $Cmca$), Ni_3ZnB_2 (space group: $C2/m$), Ni_2ZnB (space group: $C2/m$), and Ni_3Zn_2B (space group: $C2/m$)^{20-23,33}. Out of all these phases, only Ni_2ZnB and Ni_3ZnB_2 have layered structures^{20,21} with a general chemical composition ($Ni_{n+1}ZnB_n$) like the MAX phases ($M_{n+1}AX_n$). In these two layered MAB structures, beside the expected Ni-Zn and Ni-B bonding interactions, Zn and B atoms also significantly interact leading to wave-like arrangement of the Zinc layer in both structures (**Figure 1, left**).

The synthesis of phases in the Ni-Zn-B system is quite challenging: As the Ni-Zn-B isotherm at 800°C²⁰ suggests (**Figure S1**) Ni_2ZnB and Ni_3ZnB_2 are stable at this temperature. However, due to their small phase

areas in the isotherm, a small shift in the composition will lead to the formation of impurities based on the scalene triangles representing a three-phase equilibrium. For example, in their recent discovery of Ni_2ZnB Rogl et al. obtained a multiphase product (Ni_2ZnB , $\text{Ni}_3\text{Zn}_2\text{B}$, $\text{Ni}_2\text{Zn}_{11}$)²⁰. The same authors previously synthesized single-phase Ni_3ZnB_2 by mixing NiB_x master alloy with fine Zn filings in proper compositional ratio. The mixture was then submitted to several preparation steps (milled/cold-pressed/heat-treated/annealed/quenched/re-milled/hot-pressed) that enabled the synthesis of a polycrystalline sample with isotropic particles (no preferred orientation observed)²³. We have developed a new approach in our synthesis, by first preparing a high quality Ni_2B master alloy through arc-melting as it melts congruently (**Figure S2**). Ni_2B was then powdered and mixed with the remaining elements according to the targeted composition, pressed to a pellet and submitted to a melting-solidification technique including pre-alloying and heat treatments with regrinding steps (see the detailed procedure given in the supporting information and the temperature profiles in **Figure S3**). This synthesis method led to the formation of highly anisotropic particles of Ni_2ZnB and Ni_3ZnB_2 , as proven by the following analysis. Rietveld refinements (**Figure 1**) of the powder X-ray diffraction (PXRD) patterns were conducted on both products. Severe intensity mismatches (**Figure S4**) were initially observed mainly for the $00l$ reflections, but they were successfully corrected using preferred orientation refinement along the c -axis, hinting at layered morphologies of the two samples. Indeed, high-resolution scanning electron microscopy (HRSEM) images of the bulk Ni_2ZnB and Ni_3ZnB_2 products showed highly stacked thin sheets (**Figures 2a, 2b and S5**). The PXRD refinement results confirmed the expected crystal structures and no impurity peaks were detected, hinting at almost single-phase syntheses, but SEM backscattering imaging detected small Ni-rich impurity inclusions in the samples (see **Figure S6**). Energy dispersive X-ray spectroscopy (EDS) through elemental mapping confirmed the presence of all elements and their homogeneous distribution in both samples (**Figures S5 and S6**). Inductively coupled plasma (ICP) spectroscopy measurements provided a Ni:Zn ratio of 3.16:1 and 2.20:1 for Ni_3ZnB_2 and Ni_2ZnB , respectively. The slight deviation of the ICP results from the ideal Ni:Zn ratios is likely due to the Ni-rich impurity inclusions mentioned above. Furthermore, selected area electron diffraction (SAED) from a transmission electron microscopy (TEM) image of a Ni_3ZnB_2 thin particle confirmed its crystallinity with diffraction peaks indexed according to its crystal structure (space group $C2/m$, **Figure S7**).

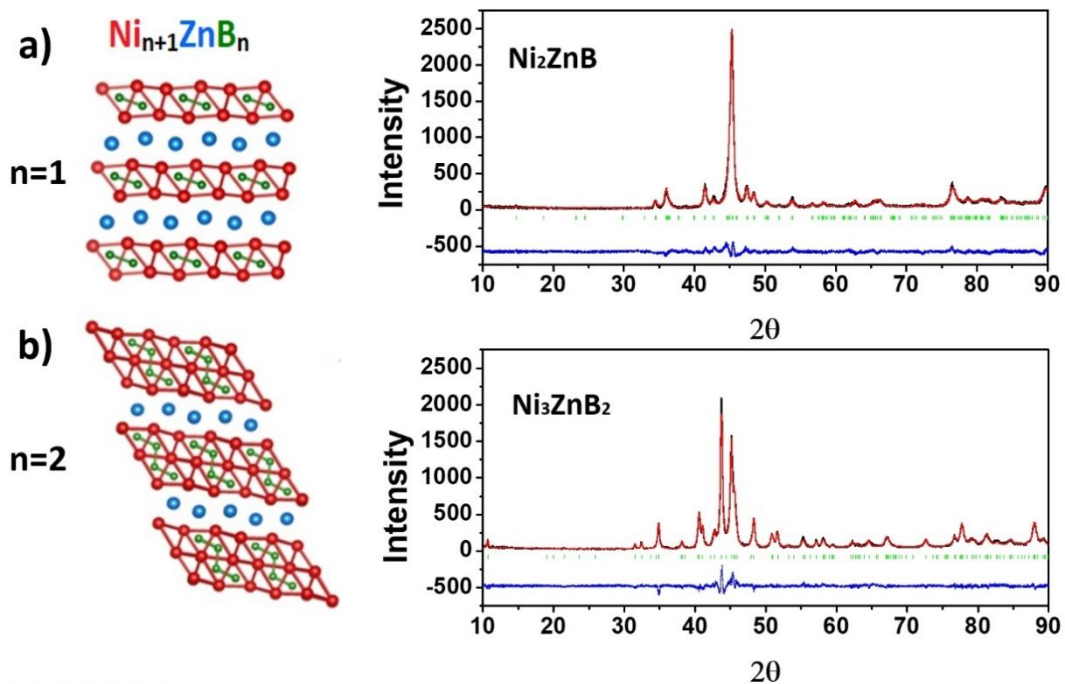


Figure 1. Crystal structures and Rietveld refinements of the powder XRD patterns of Ni_2ZnB (a) and Ni_3ZnB_2 (b). The red and the black curves represent the measured and the calculated patterns, respectively, whereas the blue curves show the intensity difference. The positions of the Bragg peaks are shown in green.

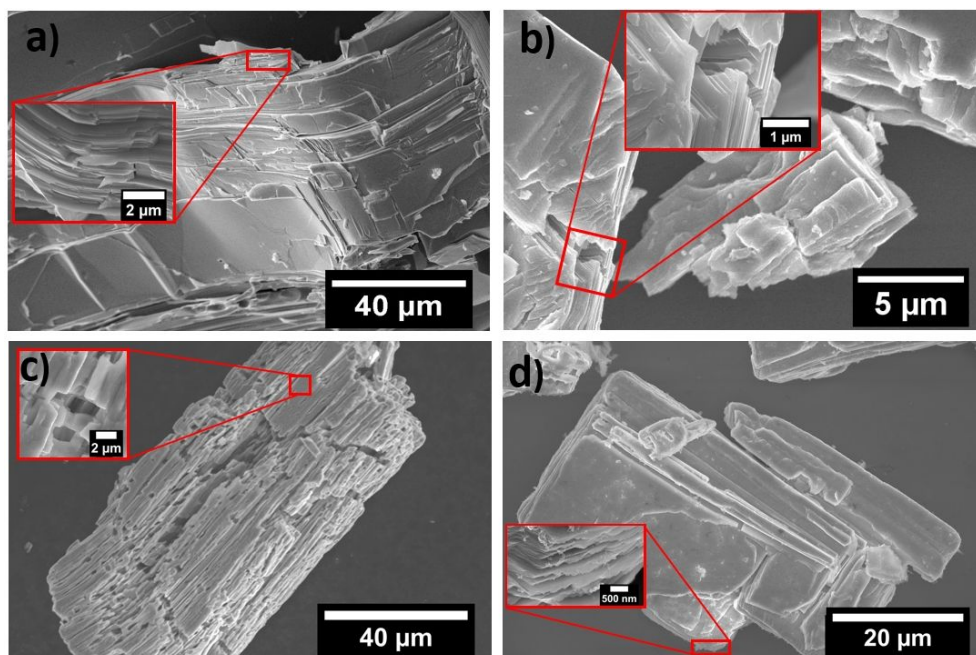


Figure 2. SEM images of the as-synthesized (a and b) and the 72hr HCl-etched (c and d) samples of Ni_2ZnB (a, c) and Ni_3ZnB_2 (b, d).

To investigate the possible Zn etching from Ni_2ZnB and Ni_3ZnB_2 bulk samples, several etchants (HCl, NaOH and FeCl_3/HCl) were tried (see supporting information for details). We found that only 1M HCl had the most promising results. The Ni_2ZnB and Ni_3ZnB_2 bulk samples were powdered and treated with 1M HCl acid for 72 hours. The prepared solutions were regularly shaken and ultrasonicated every 8 hours for about 3 minutes. Ultrasonication broke the bulk crystals into small pieces thereby accelerating the acid etching. After 72 hours, most of the sample had precipitated, leaving an almost colorless solution, an indication that a complete Zn removal, as observed in the case of Al etching in MAX phases such as $\text{Ti}_{n+1}\text{AlC}_n$, has not occurred. Instead, very small amounts of etched materials were obtained, and our preliminary analysis suggests that they contain less Zn than the bulk and the precipitated samples, thereby hinting at only partial etching (results to be communicated elsewhere), as observed in recent etching studies on Al-based MAB phases^{26, 27, 34}. The acid-treated Ni_2ZnB and Ni_3ZnB_2 precipitates were investigated by PXRD, SEM, EDS, and ICP. According to PXRD, the Ni_2ZnB and Ni_3ZnB_2 samples remained crystalline and their crystal structures did not change during the etching process (**Figure S8**). However, their morphologies were affected, as shown by SEM images in **Figures 2c** and **2d**: SEM analysis of the etched Ni_2ZnB crystals shows that the top sheets were attacked by HCl leading to the emergence of pores and layer openings (**Figures 2c and S9**). The pore sizes ranged from 100 nanometers to a few micrometers. The SEM analysis of etched Ni_3ZnB_2 crystals indicated that the top sheets were not attacked by the acid, as only the layer openings were observed (**Figure 2d**). This finding reveals that Ni_3ZnB_2 has more robust layers than Ni_2ZnB , which may be due to the thickness differences of the Ni-B slabs (**Figure 1, left**). Since our chemical analysis (see SI) showed the same composition between these precipitates and the unetched samples, we hypothesize that the layer opening observed after etching is due to the ultrasonication. We are currently carrying out further ultrasonication experiments in different solutions to verify this hypothesis.

The BET surface areas of etched Ni_2ZnB and Ni_3ZnB_2 are $95.9 \text{ m}^2 \text{ g}^{-1}$ and $0.7 \text{ m}^2 \text{ g}^{-1}$, respectively. The pristine materials did not produce meaningful BET values, with the best measurement leading to a negligible value of $0.03 \text{ m}^2 \text{ g}^{-1}$, indicating orders of magnitude improvement of the surface area after the acid treatment. After etching, the newly exposed surfaces are believed to be terminated by hydroxide or oxide groups like in MXenes.⁹⁻¹² These surface species are capable of reversible redox reactions, thus interesting electrochemical properties relevant to battery materials can be expected. We have therefore examined the etched MAB phases in Li-ion half-cells using Li foil as the counter electrode. The MAB electrode was composed of 80 wt.% of Ni_2ZnB (or Ni_3ZnB_2), 10 wt.% of polyvinylidene difluoride (PVDF) as binder, and 10 wt.% of acetylene black as the conductive additive. **Figure 3a** shows the cycle stability and coulombic efficiency (CE) under various lithiation-delithiation rates of 20 mA g^{-1} , 100 mA g^{-1} and 300 mA g^{-1} . At 20 mA g^{-1} , the first lithiation capacity of Ni_2ZnB electrode was approximately 180 mAh g^{-1} and a reversible capacity of $\sim 110 \text{ mAh g}^{-1}$ was achieved. At higher rates, the reversible capacities were ~ 90

mAh g⁻¹ at 100 mA g⁻¹ and ~70 mAh g⁻¹ at 300 mA g⁻¹. The first cycle coulombic efficiency (CE) was 49.2% at 20 mA g⁻¹, and the CE in the following cycles improved fast to an average value of 99.3 %. In all the specific capacity measurements, Ni₂ZnB demonstrated a 20 mAh g⁻¹ (at 100 mA g⁻¹) higher specific capacity than Ni₃ZnB₂ (**Figure 3a, middle**), which is likely due to the higher surface area of etched Ni₂ZnB. Both materials demonstrate excellent cycle stability with a slight incremental trend of capacity, which most probably results from accessibility of Li ions to active sites that has improved upon cycling.³⁵ The powder XRD analysis of the MAB phases after the first lithiation and delithiation (**Figure S8**) shows that the crystal structures of Ni₂ZnB and Ni₃ZnB₂ are retained. However, the intensity of the peaks significantly decreased, indicating that the crystallinity is reduced in these materials upon electrochemical reaction with Li. The representative lithiation-delithiation potential curves and cyclic voltammograms (CV) are shown in **Figure 3 (b-e)**, and both methods indicate significant irreversibility in the first cycle (leading to low initial CE), a behavior also reported for similar materials such as MXenes and their composites.^{9,10} To understand the origin of the irreversible capacity, the oxidation states of the surface elements were analyzed by X-ray photoelectron spectroscopy (XPS) after the acid etching, the first lithiation, and the first delithiation. As shown in **Figure 4a**, the Ni species on the surface of Ni₂ZnB after etching include metallic Ni (Ni 2p_{3/2} at 852.6 eV), Ni²⁺ (Ni 2p_{3/2} at 854.0 eV), and Ni³⁺ (Ni 2p_{3/2} at 855.6 eV). After the first lithiation the Ni³⁺ species was completely reduced to lower oxidation state. The Ni²⁺ species was also significantly reduced (using the peak of metallic Ni as the standard). After the delithiation, Ni³⁺ species re-emerged, however, the lower peak intensity relative to the etched sample indicates that the redox reaction of nickel is not completely reversible in the first cycle. The Zn species (**Figure 4b**) on the surface of etched Ni₂ZnB show two states including metallic Zn (Zn 2p_{3/2} at 1021.9 eV) and an oxidized state (Zn 2p_{3/2} at 1026.3 eV). After the first lithiation, the oxidized Zn is completely reduced to the metallic state, and this reduction process is irreversible indicated by the XPS Zn 2p spectrum after the delithiation. As displayed in **Figures 4c and 4d**, the Ni and Zn surface species on Ni₃ZnB₂ show the same behavior as observed in Ni₂ZnB. The surface boron species in both compounds are inert as indicated by their XPS B 1s spectra (**Figure S10**). Therefore, we suggest that the electrochemical redox reactions of Ni species on the surface contribute to the electrochemical performance of these two MAB phases. The irreversible reduction of Ni and Zn species in the first cycle is a major cause for the low initial CE in addition to the possible side reactions of solid electrolyte interphase formation.

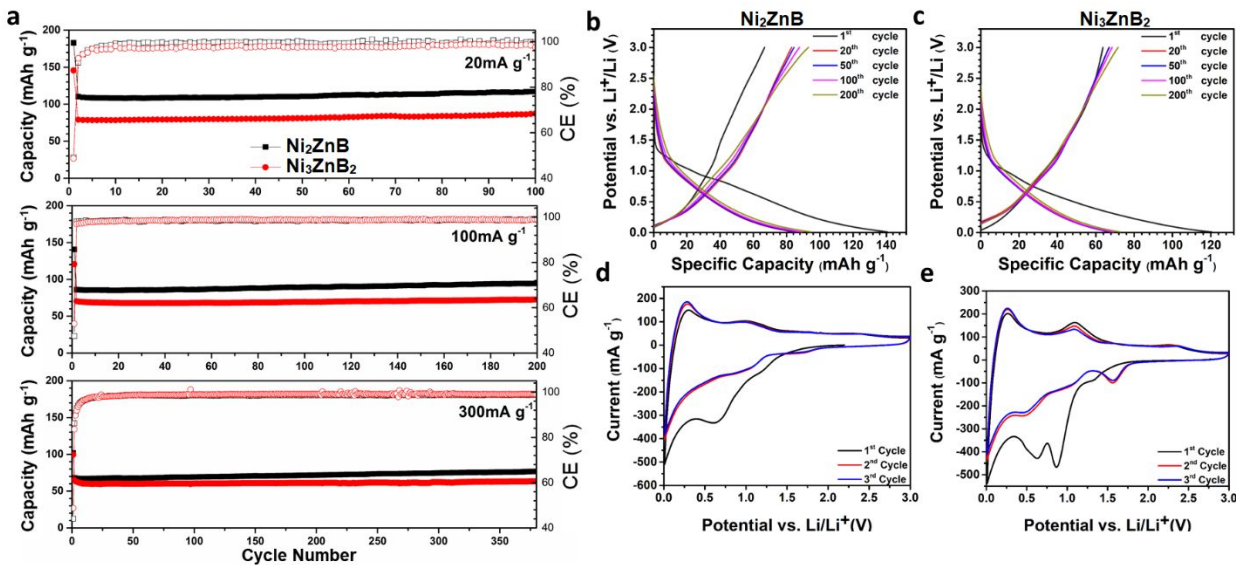


Figure 3. Electrochemical characterizations of Ni_2ZnB and Ni_3ZnB_2 electrodes. (a) Cycle stability of Ni_2ZnB and Ni_3ZnB_2 at various current rates; Representative lithiation and delithiation curves of (b) Ni_2ZnB and (c) Ni_3ZnB_2 at the rate of 100 mA g^{-1} ; Cyclic voltammetry of (d) Ni_2ZnB and (e) Ni_3ZnB_2 at 1 mV s^{-1} scan rate from 0.01 to 3.0 V vs Li/Li^+ .

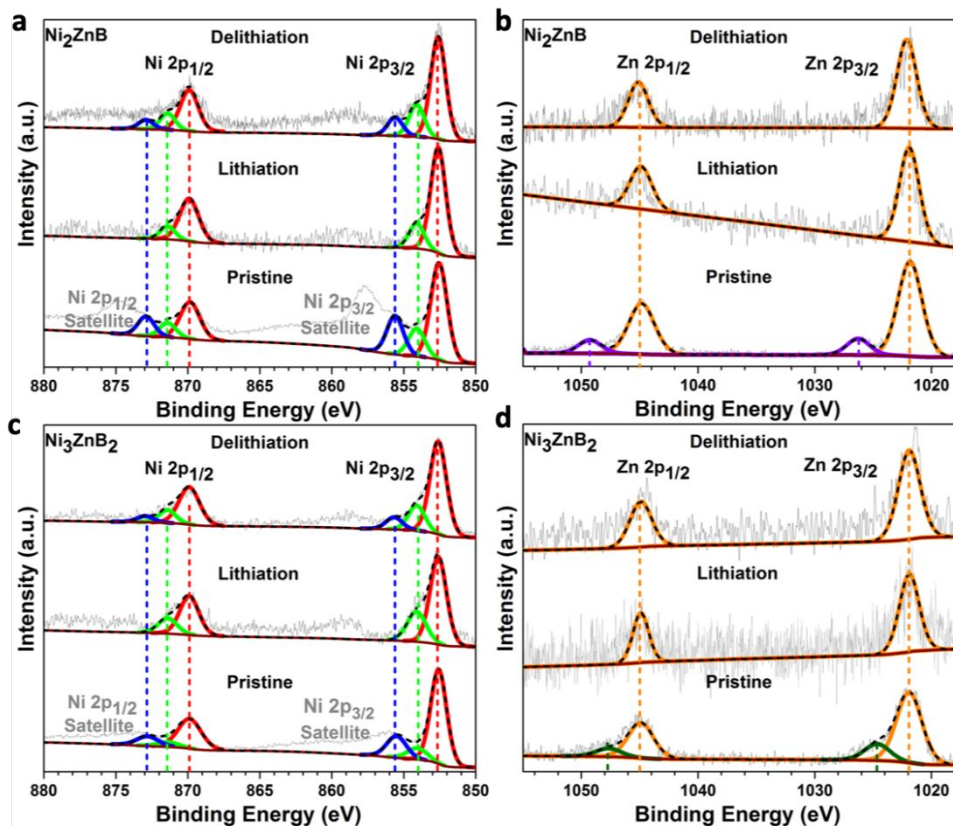


Figure 4. XPS Ni 2p and Zn 2p spectra of Ni_2ZnB (a, b) and Ni_3ZnB_2 (c, d) after acid etching (pristine) and after the first lithiation-delithiation cycle.

Conclusions

In this study, the syntheses of the MAB phases $\text{Ni}_{n+1}\text{ZnB}_n$ ($n = 1, 2$) were systematically investigated. The synthesized MAB phases were exposed to dilute HCl in order to study the effect of etching on their crystal structure. It was seen that the proposed MAB phases get partially attacked by the acid and form pores and sheet openings. The battery performances of the unetched and etched MAB phases were investigated. While the bulk Ni_2ZnB and Ni_3ZnB_2 were not active, the etched phases showed a capacity of $\sim 90 \text{ mAhg}^{-1}$ and $\sim 75 \text{ mAhg}^{-1}$, respectively. XPS and BET analyses suggest that increased surface area and electrochemical redox reactions of surface Ni species are responsible for the drastic change in battery performances. Future works should focus on increasing the surface area of these and other MAB phases containing elements that can undergo redox reactions toward applications in various metal-ion batteries.

Acknowledgements

This work was supported by the startup fund to BPTF at UC Riverside and the National Science Foundation Career award to BPTF (no. DMR-1654780). The CFAMM center at UC Riverside for electron microscopy and microanalysis.

References:

1. Barsoum M, El - Raghy T. Synthesis and characterization of a remarkable ceramic. Ti_3SiC_2 . 1996;79(7):1953-6.
2. Jeitschko W, Nowotny Ht, Benesovsky F. Carbides of formula T_2MC . Journal of the Less Common Metals. 1964;7(2):133-8.
3. Schuster J, Nowotny H, Vaccaro C. The ternary systems: CrAlC, VAlC, and TiAlC and the behavior of H-phases (M_2AlC). Journal of Solid State Chemistry. 1980;32(2):213-9.
4. Barsoum MW, El-Raghy T. The MAX phases: Unique new carbide and nitride materials: Ternary ceramics turn out to be surprisingly soft and machinable, yet also heat-tolerant, strong and lightweight. American Scientist. 2001;89(4):334-43.
5. Khazaei M, Arai M, Sasaki T, Estili M, Sakka Y. Trends in electronic structures and structural properties of MAX phases: a first-principles study on M_2AlC ($\text{M} = \text{Sc, Ti, Cr, Zr, Nb, Mo, Hf, or Ta}$), M_2AlN , and hypothetical M_2AlB phases. J Phys: Condens Matter. 2014;26(50):505503.
6. Barsoum M, El-Raghy T, Ali M. Processing and characterization of Ti_2AlC , Ti_2AlN , and $\text{Ti}_2\text{AlC}_{0.5}\text{N}_{0.5}$. Metallurgical and Materials Transactions A. 2000;31(7):1857-65.
7. Barsoum M, El-Raghy T. Room-temperature ductile carbides. Metallurgical and Materials Transactions A. 1999;30(2):363-9.
8. Naguib M, Kurtoglu M, Presser V, Lu J, Niu J, Heon M, et al. Two - dimensional nanocrystals produced by exfoliation of Ti_3AlC_2 . Adv Mater. 2011;23(37):4248-53.
9. Zhao MQ, Ren CE, Ling Z, Lukatskaya MR, Zhang C, Van Aken KL, et al. Flexible MXene/carbon nanotube composite paper with high volumetric capacitance. Adv Mater. 2015;27(2):339-45.

10. Naguib M, Come J, Dyatkin B, Presser V, Taberna P-L, Simon P, et al. MXene: a promising transition metal carbide anode for lithium-ion batteries. *Electrochemistry Communications*. 2012;16(1):61-4.
11. Liang X, Arnd Garsuch, and Linda F. Nazar. Sulfur cathodes based on conductive MXene nanosheets for high - performance lithium - sulfur batteries. *Angewandte Chemie International Edition*. 2015;54(13):3907-11.
12. Lukatskaya MR, Mashtalir O, Ren CE, Dall'Agnese Y, Rozier P, Taberna PL, et al. Cation intercalation and high volumetric capacitance of two-dimensional titanium carbide. *Science*. 2013;341(6153):1502-5.
13. Shahzad F, Alhabeab M, Hatter CB, Anasori B, Hong SM, Koo CM, et al. Electromagnetic interference shielding with 2D transition metal carbides (MXenes). *Science*. 2016;353(6304):1137-40.
14. Ade M, Hillebrecht H. Ternary borides Cr_2AlB_2 , Cr_3AlB_4 , and Cr_4AlB_6 : The first members of the series $(\text{CrB}_2)_n \text{CrAl}$ with $n= 1, 2, 3$ and a unifying concept for ternary borides as MAB-phases. *Inorganic chemistry*. 2015;54(13):6122-35.
15. Zhou Y, Xiang H, Dai F-Z, Feng Z. Electrical conductive and damage-tolerant nanolaminated MAB phases Cr_2AlB_2 , Cr_3AlB_4 and Cr_4AlB_6 . *Mater Res Lett*. 2017;5(6):440-8.
16. Zhou Y, Xiang H, Dai F-Z, Feng Z. $\text{Cr}_5\text{Si}_3\text{B}$ and $\text{Hf}_5\text{Si}_3\text{B}$: New MAB phases with anisotropic electrical, mechanical properties and damage tolerance. *Journal of Materials Science & Technology*. 2018;34(8):1441-8.
17. Kota S, Zapata-Solvas E, Ly A, Lu J, Elkassabany O, Huon A, et al. Synthesis and characterization of an alumina forming nanolaminated boride: MoAlB . *Scientific reports*. 2016;6:26475.
18. Petry K, Jung W. Ternäre Boride der Rutheniums mit Aluminium und Zink. *Z Kristallogr*. 1988;182:153.
19. Zhou Y, Xiang H, Dai FZ, Feng Z. $\text{Y}_5\text{Si}_2\text{B}_8$: A theoretically predicted new damage - tolerant MAB phase with layered crystal structure. *J Am Ceram Soc*. 2018;101(6):2459-70.
20. Failamani F, Podlucky R, Bursik J, Rogl G, Michor H, Müller H, et al. Boron-phil and boron-phob structure units in novel borides $\text{Ni}_3\text{Zn}_2\text{B}$ and Ni_2ZnB : experiment and first principles calculations. *Dalton Transactions*. 2018;47(10):3303-20.
21. Malik ZP, Sologub O, Grytsiv A, Giester G, Rogl PF. Crystal Structure of Novel Ni–Zn Borides: First Observation of a Boron–Metal Nested Cage Unit: B_{20}Ni_6 . *Inorganic Chemistry*. 2011;50(16):7669-75.
22. Malik Z, Grytsiv A, Rogl, P Giester, G Bursik J. Phase relations and structural features in the system Ni–Zn–B. *Journal of Solid State Chemistry* 2013;198:150-61.
23. Malik Z, Grytsiv A, Michor H, Rogl G, Puchegger S, Müller H, et al. Physical properties of the ternary borides $\text{Ni}_{21}\text{Zn}_2\text{B}_{20}$ and Ni_3ZnB_2 . *J Alloys Compd*. 2013;550:302-7.
24. Guo, Z Zhu, L Zhou J, Sun Z, Microscopic origin of MXenes derived from layered MAX phases, *RSC Adv*. 2015;5:25403-8.
25. Zhang H, Xiang H, Dai F-z, Zhang Z, Zhou Y. First demonstration of possible two-dimensional MBene CrB derived from MAB phase Cr_2AlB_2 . *Journal of Materials Science & Technology*. 2018;34(11):2022-6.
26. Alameda LT, Holder CF, Fenton JL, Schaak RE. Partial etching of Al from MoAlB single crystals to expose catalytically active basal planes for the hydrogen evolution reaction. *Chemistry of Materials*. 2017;29(21):8953-7.
27. Alameda LT, Moradifar P, Metzger ZP, Alem N, Schaak RE. Topochemical deintercalation of Al from MoAlB : stepwise etching pathway, layered intergrowth structures, and two-dimensional MBene. *Journal of the American Chemical Society*. 2018;140(28):8833-40.

28. Guo Z, Zhou J, Sun Z. New two-dimensional transition metal borides for Li ion batteries and electrocatalysis. *Journal of Materials Chemistry A*. 2017;5(45):23530-5.
29. Stuart J, Lefler M, Rhodes CP, Licht S. High Energy Capacity TiB_2/VB_2 Composite Metal Boride Air Battery. *J Electrochem Soc*. 2015;162(3):A432-A6.
30. Yang H, Wang Y, Ai X, Cha C. Metal borides: competitive high capacity anode materials for aqueous primary batteries. *Electrochem Solid-State Lett*. 2004;7(7):A212-A5.
31. Manthiram A, Knight JC, Myung ST, Oh SM, Sun YK. Nickel - rich and lithium - rich layered oxide cathodes: progress and perspectives. *Advanced Energy Materials*. 2016;6(1):1501010.
32. Nitta N, Wu F, Lee JT, Yushin G. Li-ion battery materials: present and future. *Mater Today*. 2015;18(5):252-64.
33. S Bhan SS, A Lal. The B--Ni--Zn(Boron--Nickel--Zinc) System. *Journal of Alloy Phase Diagrams(India)*. 1990;6(3):147-52.
35. Alameda LT, Lord RW, Barr JA, Moradifar P, Metzger ZP, Steimle BC, et al. Multi-Step Topochemical Pathway to Metastable Mo_2AlB_2 and Related Two-Dimensional Nanosheet Heterostructures. *Journal of the American Chemical Society*. 2019;141:10852-61.
35. Mashtalir O, Lukatskaya MR, Zhao MQ, Barsoum MW, Gogotsi Y. Amine - Assisted Delamination of Nb_2C MXene for Li - Ion Energy Storage Devices. *Advanced Materials*. 2015;27(23):3501-6.

Acid-treated $\text{Ni}_{n+1}\text{ZnB}_n$ ($n = 1, 2$) MAB phases become highly active Li-ion battery anodes.

